Supporting Information

Spectroscopic Evidence of the Salt-Induced Conformational Change around the Localized Electric Charges on the Protein Surface of Fibronectin Type III

Chikashi Ota[1], Yui Fukuda[2], Shun-ichi Tanaka[2] and Kazufumi Takano[2,*]

[1] College of Life Sciences, Ritsumeikan University, Kusatsu, Shiga 525-8577, Japan

[2] Department of Biomolecular Chemistry, Kyoto Prefectural University, Sakyo-ku, Kyoto 606-8522, Japan

* Corresponding author

E-mail address: takano@kpu.ac.jp

Tel/Fax: +81-75-703-5654

ORCID iD: 0000-0002-7548-7314

Supporting Information 1

FN3 has one Trp residue located at residue 22, one Phe at residue 48, and six Tyr at residues 31, 32, 36, 68, 73, and 92.[1-3] Glu^{47} is located just next to Phe^{48}.

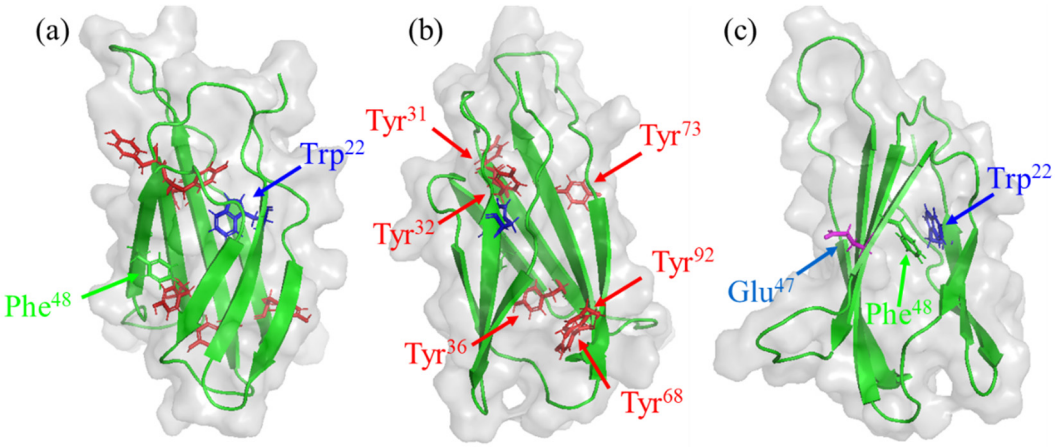

Figure S1. Internal positions of (a) Trp^{22} (a blue arrow), Phe^{48} (a green arrow), (b) six Tyr (red arrows) residues and (c) Glu^{47} (a magenta arrow) of FN3 protein.

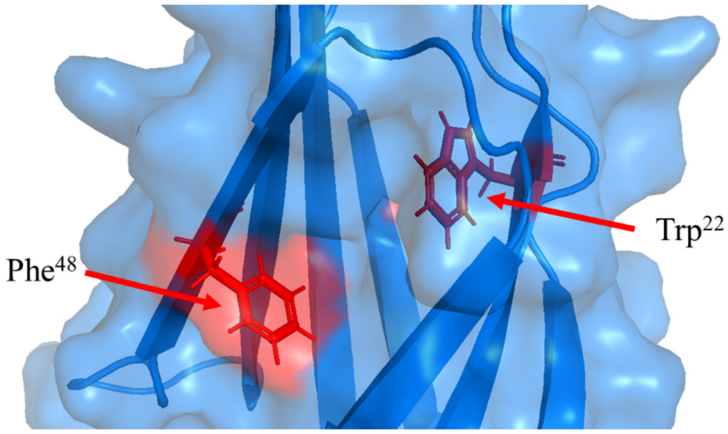

Figure S2. Solvent accessible surface area of Trp^{22} and Phe^{48} (red color). Trp^{22} is the highly conserved residue in FN3 with small solvent accessible surface area (SASA; 1 %), while Phe^{48} is located near the protein surface with a relatively high SASA (41 %).[3]

Supporting Information 2

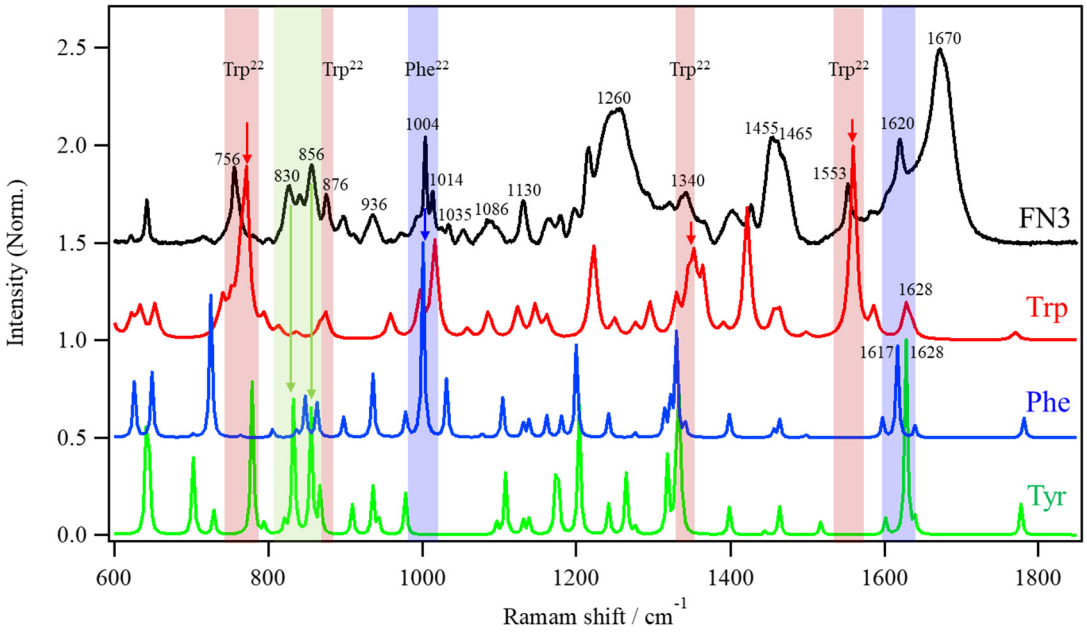

Figure S3. The Raman spectrum of FN3 (200 mg/mL) at pH 6.0 (black line) and calculated Raman spectra of Trp (red line), Phe (blue line) and Tyr (green line) at the B3LYP/6-311++G(d, p) level of therory as references.

Raman shift / cm^{-1}	Functional group	Assignment
1670	Amide backbone	C=O streching with hydrogen bonding interaction (Amide I)
1628	Trp	Phenyl ring vibratioin
1628	Tyr	In plane ring strech
1617	Phe	In plane ring strech
1553	Trp	Symmetric naphthalene type streching
1465	CH_3	CH_3 deformation
1455	CH_2	CH_2 deformation
1340	Trp	In plane pyrrole ring vibration with a out of plane vibration
1260	Amide backbone	CN stretching coupled with NH bending (Amide III)
1130	Trp	NH_3^+ rocking with indole ring side chain stretching
1086	Trp	C_β-C_γ and indole ring stretching
1035	Phe	In plane CH bend of benzene ring
1014	Trp	Benzene and pyrrole ring breathing out-of-phase
1004	Phe	Ring breathing mode of benzene ring
936	Amide backbone	α-helix backbone C-C_α-N stretching
876	Trp	Skeletal vibration with appreciable NH pyrrole bend
856	Tyr	Symmetric in-plane ring breathing (Y5)
830	Tyr	Fermi resonance band between Y5 and the first overtone of an out-of-plane mode
756	Trp	Benzene and pyrrole ring breathing in-phase

Table S1. Spectral assignment of each Raman band in FN3 protein from Refs 4-11.

Figure S3 shows the Raman spectrum of FN3 (200 mg/mL) at pH 6.0 and calculated Raman spectra of Trp, Phe and Tyr at the B3LYP/6-311++G(d, p) level of therory as references, which has provided reliable theoretical data for various amino acids.[9,10,12,13] Quntum mechanical calculations were carried out by means of Firefly package.[14,15] The spectral assignment of each Raman band in FN3 protein based on the previous experimental studies of proteins and amino acids is summarized in Table S1.[4-11] The spectral assignment of each Raman band coincides well with the calculated results, indicating that the Raman bands are properly assigned from both the previous experimental studies and calculated results.

Supporting Information 3

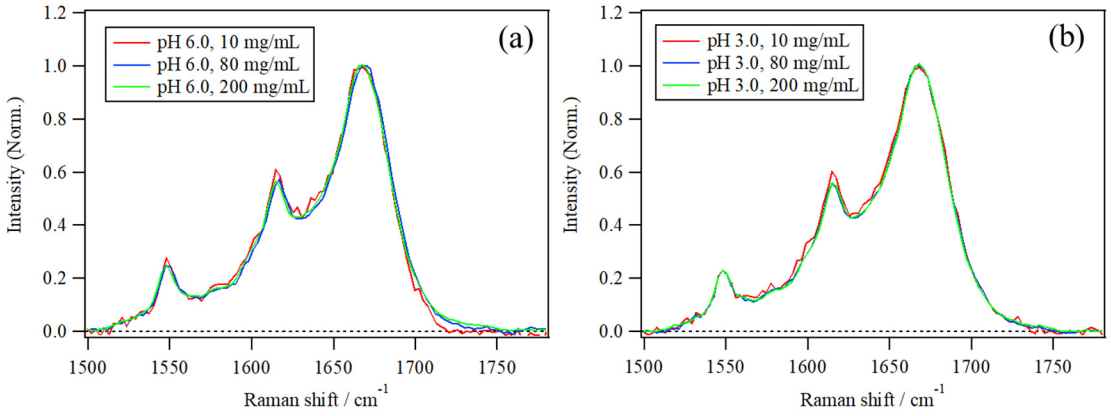

Figure S4. Protein concentration dependences of the amide I band of FN3 at (a) pH 6.0 and (b) pH 3.0.

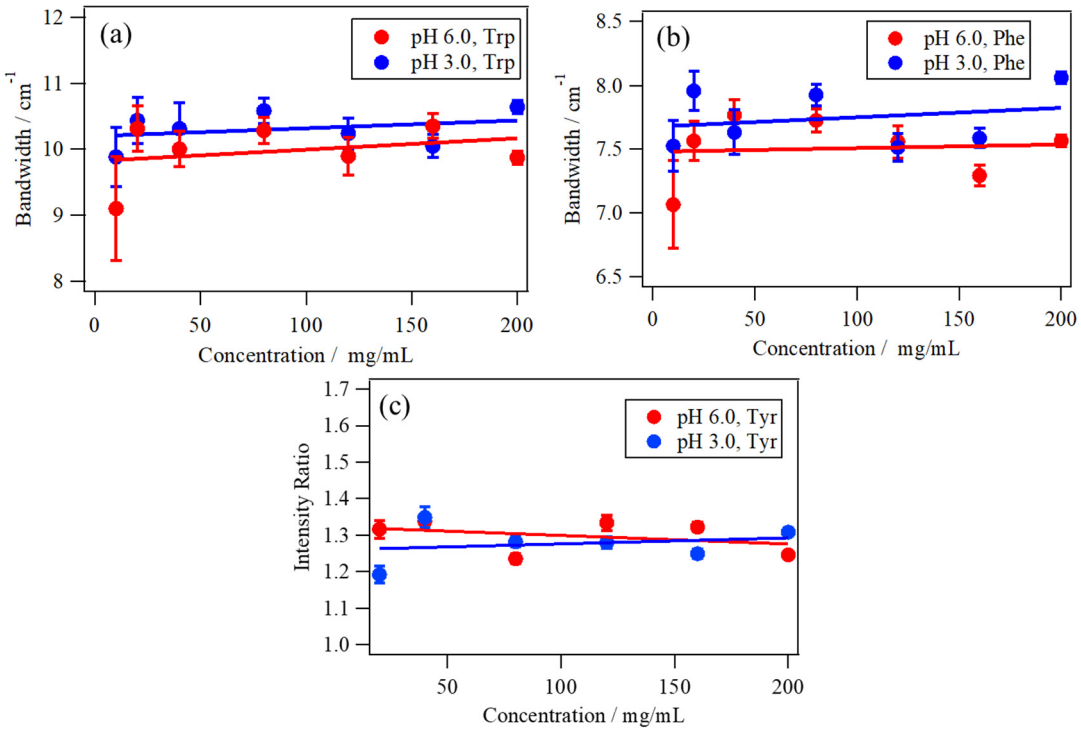

Figure S5. Protein concentration dependences of the bandwidth of (a) the Trp band at 1553 cm^{-1}, (b) Phe band at 1004 cm^{-1} and (c) Tyr doublet intensity ratio (I_{856}/I_{830}) of FN3 at pH 6.0 (red circles) and pH 3.0 (blue circles). Error bars are the standard deviation of the fluctuations of the bandwidth and the band intensity ratio due to the shot noise.

To ascertain the concentration-dependent change of the secondary structure and the local conformational changes in the Trp, Phe, and Tyr residues, which are induced by the protein-protein interactions of the FN3 proteins, the measurement of FN3 concentration dependence was performed using Raman spectroscopy over a wide concentration range from 10 to 200 mg/mL. Figure S4 shows the amide I bands of FN3 (10, 80, and 200 mg/mL) at (a) pH 6.0 and (b) pH 3.0. The amide I bands of each concentration almost overlapped. The results indicated that there is no significant change in the secondary structure by the concentration-induced protein-protein interactions. Figure S5a and b show the concentration dependence of the bandwidth of (a) the Trp band at 1553 cm^{-1} and (b) the Phe band at 1004 cm^{-1} at pH 6.0 and pH 3.0. The bandwidth of Trp and Phe at both pH conditions was almost constant during the concentration change, indicating that the local conformation around Trp and Phe is not affected by the concentration change. Especially, Trp^{22}, which is the only one Trp residue in FN3, is conserved at the hydrophobic core. Thus, the environment around the hydrophobic core is almost unaffected by the concentration change. Figure S5c shows the concentration dependence of the Tyr doublet intensity ratio (I_{856}/I_{830}) of FN3 at pH 6.0 and pH 3.0. Siamwiza and colleagues suggested that Tyr residues have a doublet band at approximately 830 and 850 cm^{-1}, which is caused by a Fermi resonance effect between the in-plane fundamental mode and the first overtone of a phenol ring out-of-plane mode located at approximately 413 cm^{-1}. Based on the results of pH and the solvent effects on the Fermi doublet of the p-cresol and its derivatives as a model system, the Tyr doublet ratio (I_{850}/I_{830}) can be a marker of the hydrogen-bonding environment.[16] The Tyr doublet intensity ratios (I_{856}/I_{830}) of FN3 at pH 6.0 and pH 3.0 remained almost constant over the concentration range, indicating that the hydrogen-bonding environment around the Tyr residues of FN3 is not

affected by the concentration-induced protein-protein interactions. Since FN3 has six Tyr residues both inside and on the surface of the protein, these results could indicate that the hydration environment of the overall protein is not affected by the concentration change.

The collective protein concentration dependence of the amide I band, the Trp and Phe bandwidth, and Tyr doublet intensity ratio remained almost unchanged at the different concentrations, indicating that there is no specific change in both the overall and local protein conformation and their hydration environment. In other words, specific protein-protein interaction does not occur, even in the highly concentrated region.

Supporting Information 4

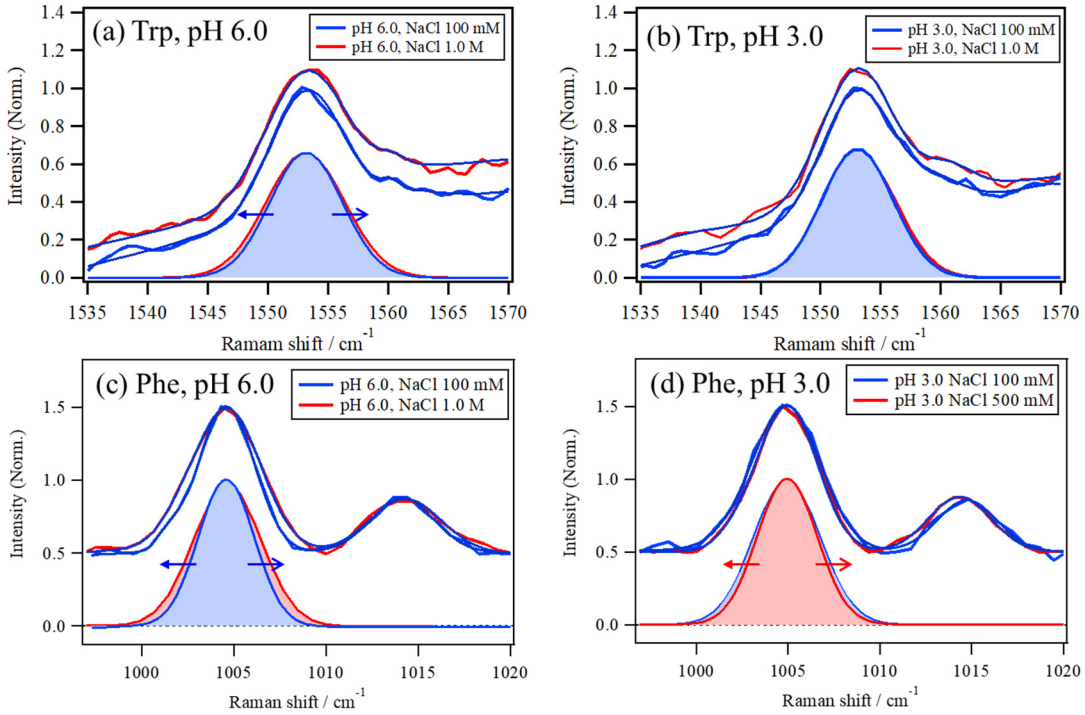

Figure S6. Trp bands and their Gaussian-Lorentz fitting results (purple line) of FN3 at (a) pH 6.0 and (b) pH 3.0 with the NaCl concentration at 100 mM and 1.0 M. Phe bands and their Gaussian-Lorentz fitting result (purple line) of FN3 at (c) pH 6.0 with the NaCl concentration at 100 mM and 1.0 M at (d) pH 3.0 with the NaCl concentration at 100 mM and 500 mM.

Trp and Phe bands of FN3 at pH 6.0 and 3.0 and the Gaussian-Lorentz fitting results (purple line) are shown in Figure S6. The bandwidths of Trp (7.7 cm^{-1}) and Phe (4.3 cm^{-1}) at pH 6.0 with 1.0 M NaCl are broadening compared to the one of Trp (7.1 cm^{-1}) and Phe (3.6 cm^{-1}) with 100 mM NaCl. On the other hand, the bandwidth of Trp (7.0 cm^{-1}) at pH 3.0 with 100 mM NaCl is almost the same as the one (7.1 cm^{-1}) with 1.0 M NaCl and the bandwidth of Phe (4.3 cm^{-1}) at pH 3.0 with 100 mM NaCl is larger than the one (3.8 cm^{-1}) with 500 mM NaCl.

Supporting Information 5

The original equation for ion–protein interaction using the relationship between the cloud-point temperature of the protein and adding salt concentration is

$$F = \frac{[M]e^{-e\psi_0/kT}}{K_d+[M]e^{-e\psi_0/kT}} \quad \text{(S1)}$$

where F is the fraction of bound sites, K_d is the surface dissociation constant, $[M]$ is the molar concentration of salt and ψ_0 is the potential at the protein surface.[17] This equation is theoritically derived based on the Gouy-Chapman-Stern theory.[18] The neutralization of surface chages by ion binding will reduce the electrostatic repulsion between protein moelcules and induce the protein aggregation, resulting in the rise of the cloud-point temperature. The extent of the interaction is related to the fraction of neutralization sites, F. Therefore, ion binding effects on the cloud-point temperature, T, through the addition of salt can be modeled by a Langmuir-type biniding isotherm that includes an exponential factor to account for electrostatic neutralization:

$$T = \frac{B_{max}[M]e^{-b[M]}}{K_d+[M]e^{-b[M]}} \quad \text{(S2)}$$

B_{max}, has the units of temperature and shows the maximum increase in the cloud-point temperature when all of the positive charges on the protein surface are neutralized.[17] The constant, b, has units of reciprocal molarity and is an electrostatic interaction factor and $b[M]$ is the protein surface potential. However, the fitting result using the above eqution is practically poor, because the actual relationship between electrolyte concentration and surface potential is complex, thus, a liner term and a constat is phenomenologically necessary to be added to the above equation, leading to the practically useful equation:

$$T = T_0 + \frac{B_{max}[M]e^{-b[M]}}{K_d+[M]e^{-b[M]}} + c[M] \quad \text{(S3)}$$

In the case of this current study, the bandwidth of Trp, w, is directly related to the fraction

of neutralized sites, F, because the Trp bandwidth is correlated to the protein conformation around Trp.[17] Therefore, F can be replaced with w as is the case of the cloud-point temperature, T, leading to the equation (1):

$$w = w_0 + \frac{w_{max}[M]e^{-b[M]}}{K_d + [M]e^{-b[M]}} + c[M] \quad (1)$$

Supporting Information 6

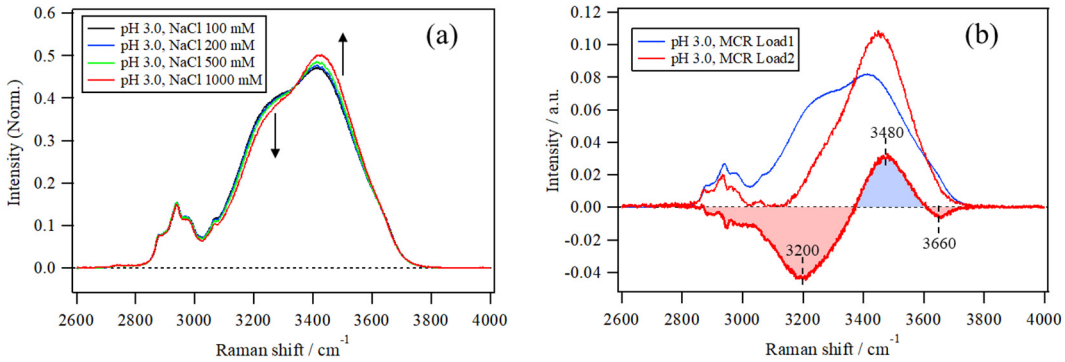

Figure S7. (a) NaCl concentration dependence (100, 200, 500 and 1000 mM) of water Raman bands at pH 3.0. (b) The MCR loadings of the concentration dependent change of the spectra at pH 3.0 and their differential loading (colored-filled line) by subtracting the 1st loading from the 2nd one.

Supporting Information 7

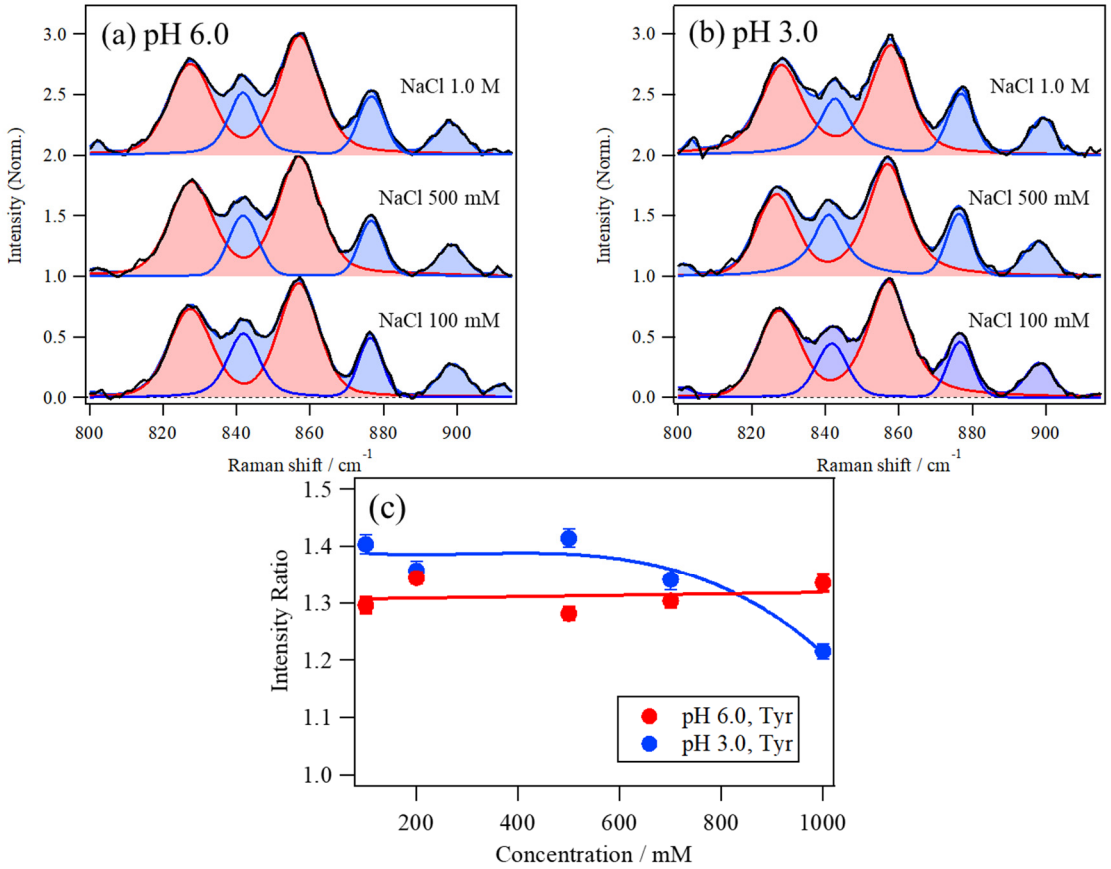

Figure S8. NaCl concentration dependences of the Tyr triplet bands of FN3 at (a) pH 6.0, (b) pH 3.0 and (c) the intensity ratio (I_{856}/I_{830}) at pH 6.0 (red circles) and (b) pH 3.0 (blue circles). Error bars are the standard deviation of the fluctuations of the band intensity ratio due to the shot noise.

To obtain knowledge of the environment surrounding the protein, the effect of NaCl concentration on the Tyr doublet ratio (I_{856}/I_{830}) of the six Tyr residues around the protein was analyzed in detail. Figure S8 shows the NaCl concentration dependence of the Tyr triplet bands of FN3 at (a) pH 6.0 and (b) pH 3.0 and (c) the intensity ratio (I_{856}/I_{830}) at pH 6.0 and 3.0. The Tyr doublet ratio (I_{856}/I_{830}) at pH 6.0 remained almost the same at the

different NaCl concentrations, indicating that the hydrogen-bonding environment around the Tyr residues is not affected by the change in NaCl concentration. In contrast, the Tyr doublet ratio at pH 3.0 was almost constant, whereas the ratio decreased at concentrations over 700 mM. These results indicate that increasing NaCl concentration can change the hydration environment of Tyr residues.

Residues of the overall FN3 protein can be more exposed to water molecules and dissociated ions at pH 3.0 than at pH 6.0 owing to the loosened structure at pH 3.0. Thus, the hydrogen-bonding environment of the Tyr residues may be affected more by the addition of NaCl, resulting in the change of the Tyr doublet ratio. Since the hydrogen-bonding environment around proteins is strongly correlated with protein structure,[19,20] the hydrogen-bonding environment of the Tyr residues at pH 3.0 may have affected the subtle and gradual conformational change around Trp^{22} and Phe^{48} (Figure 4) with increasing NaCl concentrations.

Supporting Information 8

According to some previous studies, ANS binds to the external site of protein mainly through ion pair formation, especially between Arg or Lys and the sulfonate group of ANS.[21-25] In addition to ion pair interactions, van der Waals interactions and hydrophobic interactions also complementarily support the binding at the external site or the hydrophobic region. Analysis of the crystal structures of the ANS binding sites of Arg and Lys in ANS-protein complexes, as examples shown in Figure S9, reveals that the Arg side chain is positioned to more effectively interact with both -NH and $-SO_3^-$ group of ANS compared to the case of Lys side chain, indicating that Arg side chain compared to that of Lys more effectively interacts with both the -NH and $-SO_3^-$ group of ANS.[21,25]

FN3 has 5 Arg residues (Arg^6, Arg^{30}, Arg^{33}, Arg^{78} and Arg^{93}) and 3 Lys residues (Lys^{54}, Lys^{63} and Lys^{86}) at the external site of the protein. To obtain a further insight of the binding sites of FN3, molecular docking analysis was carried out, using SwissDock at http://www.swissdock.ch, which is a protein-small molecule docking web server.[26,27] SwissDock estimates the preferable binding sites of proteins based on CHARMM22 force field calculating the van der Waals and electrostatic interaction energy between the ligand and the target protein.[26,27] In addition, the solvent effect is taken into account using FACTS (Fast Analytical Continuum Treatment of Solvation) implicit solvation model[28], which implicitly considers the solvent effect under the assumption of the continuum electrostatics models that the protein is a uniform, low dielectric region, while the solvent is a featureless high dielectric medium. Although the high computational cost is required to obtain the accurate estimation of the solvation effects of individual water molecules by explicitly and more precisely modelling the solvation effect,[29,30] the implicit solvation model is cost-efficient and practically useful. Consequently, SwissDock achieves the high

success rate of the biding site prediction compared to other well-known protein docking tools.[31]

The ANS structure was optimized by calculating the most stable structure at the B3LYP/6-311++G(d, p) level of therory. The ten possible ANS binding sites were estimated by calculating the binding free energies using SwissDock, as shown in Figure S10. Among ten possible sites, the most favorable site is the domain 8 with Arg^{33}, while other sites with Arg or Lys residues are 4 domains with Arg^{6}, Arg^{30}, Arg^{78} and Lys^{54}. The remaining sites ("others") have no Arg or Lys residues and do not form the hydrogen bonding to ANS according to the simulation, indicating that the bindings can be caused by mainly through van der Waals interactions.

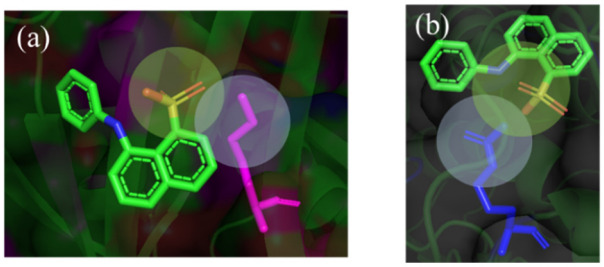

Figure S9. (a) ANS-Lys and (b) ANS-Arg complexes from crystal structures of SPE 16 (PDB: 1TXC)[21] and antibiotic target MurA (PDB: 1EYN).[21,25]

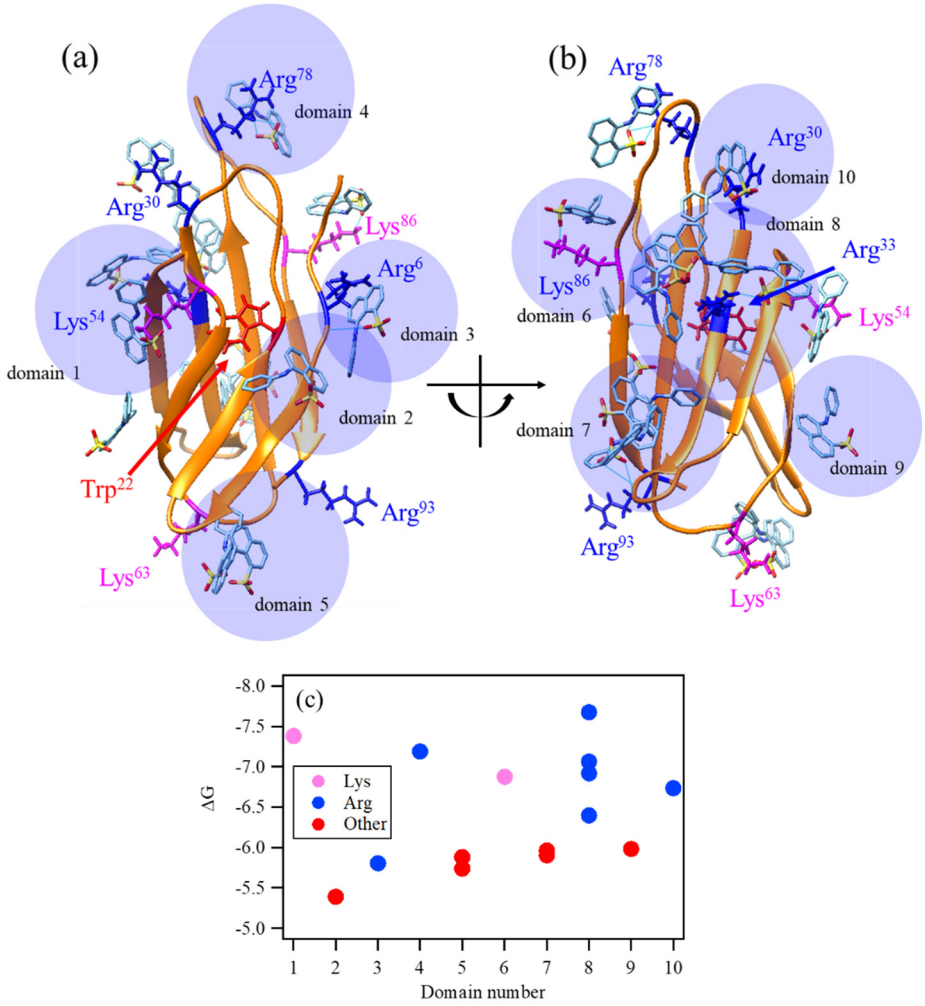

Figure S10. (a, b) ANS biding sites of FN3-ANS complexes from different angles as obtained by SwissDock, which is a protein-small molecule docking web server. (c) The estimated binding free energies of the possible binding sites.

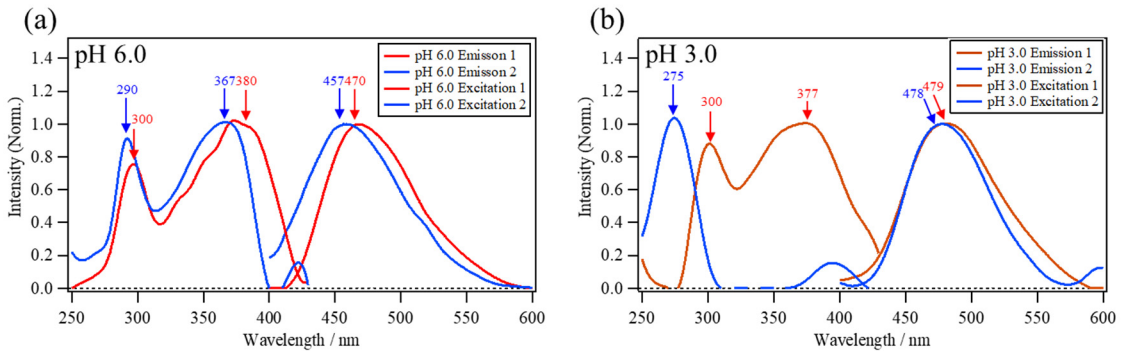

Figure S11. The MCR resolved excitation-emission spectra of ANS fluorescence in FN3 solution (1.0 mg/mL) at (a) pH 6.0 and (b) pH 3.0.

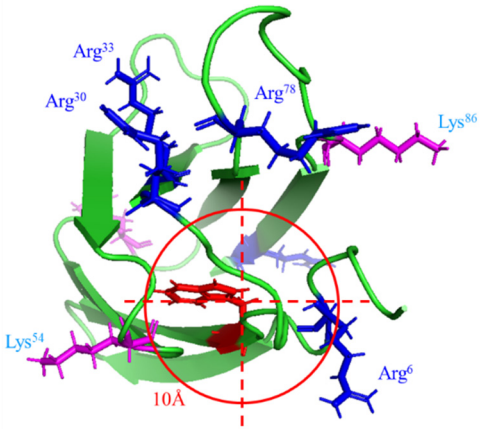

Figure S12. Distance from Trp^{22}. The red circle shows the 10 Å distance from Trp^{22}.

To experimentally characterize the binding sites of ANS at the protein surface based on the detailed hydration environment around ANS, the excitation-emission spectra of ANS fluorescence in FN3 solution (1.0 mg/mL) at pH 6.0 and 3.0 were acquired. MCR-ALS analysis of the excitation-emission spectra at pH 6.0 and 3.0 was performed to resolve the dataset. Based on the eigenvalue obtained using PCA, this dataset was resolved into two components, as shown in Figure S11a and b. The first loading at pH 6.0 corresponds to the resolved emission spectrum peaking at 470 nm. The second loading corresponds to the resolved emission spectrum peaking at 457 nm (Figure S11a). The score of 1 corresponds to the resolved excitation spectrum with a broad band at 380 nm and a sharp band at 300 nm. The score of 2 corresponds to the resolved excitation spectrum with a broad band at 367 nm and a sharp band at 290 nm. The broad excitation bands peaking at 380 and 367 nm are the ANS excitation bands. The emission bands peaking at 470 and 457 nm are the ANS emission bands.[21] Of note, the excitation spectra have sharp peaks at 290 and 300 nm, which originate from Trp absorption bands.[32,33] Trp excitation can cause ANS fluorescence, indicating energy transfer from Trp^{22} to ANS, which can be attached to Arg or Lys. Among the Arg and Lys residues, the neighboring residues within the 10 Å of Trp^{22} are Arg^{6} and Lys^{54} (Figure S12), suggesting that the fluorescence energy

transfer from Trp^{22} occurs mainly through ANS binding to Arg^{6} and Lys^{54}. Therefore, the ANS fluorescence at the Arg^{6} or Lys^{54} can be selectively observed by the excitation near 290 nm through energy transfer.

The excitation-emission spectra of ANS fluorescence in the FN3 solution at pH 3.0 were similarly analyzed as pH 6.0. The MCR loading (emission) and score (excitation) are shown in Figure S11b. The first loading at pH 3.0 has a broad band at 479 nm, and the second loading has a broad band at 478 nm, which can be similarly assigned to the ANS fluorescence bands. The score 1 (excitation) spectrum has the broad band at 377 nm with a sharp one at 300 nm, which can be also assigned to the ANS and Trp absorption bands, as is the same at pH 6.0. Of note, the excitation 2 spectrum has a sharp band at 275 nm, which can be assigned to the Tyr absorption band,[33,34] indicating that the energy transfer can occur from Trp and also from Tyr to ANS. Since FN3 has six Tyr residues around the overall protein (Figure S1b), ANS molecules not only specifically bind to the domain with Arg^{6} and Lys^{54} and but also non-specifically bind to the overall protein surface such as the domains 2, 5, 7 and 9 (Figure S10), because the positive net charge of the overall protein at pH 3.0 can easily allow the negatively charged ANS to access the protein surface and promote ANS bindings to the overall protein compared to pH 6.0. In addition, the peak position of ANS emission spectra at pH 3.0 (479 and 478 nm) is relatively red-shifted compared to that at pH 6.0 (470 and 457 nm), indicating that the hydration environment of ANS is more hydrophilic than pH 6.0.[35] In other words, the ANS molecules at pH 3.0 can be more exposed to the water molecules than those at pH 6.0, supporting the above estimation of the ANS binding sites. In contrast, the blue-shifted peak position of the ANS emission spectra at pH 6.0 indicates the hydrophobic environment of ANS, suggesting that ANS can tightly bind to the binding site around Arg

and Lys. In this manner, the binding site of ANS to the protein surface of FN3 at pH 6.0 and 3.0 can be estimated from both the molecular docking analysis and the experimental analysis of the ANS excitation-emission spectra. On the basis of these assignments, the salt effect on ANS fluorescence was analyzed from the viewpoints of both the solvation environment and the protein conformation.

Supporting Information 9

To obtain the conformational knowledge of the salt effect on FN3 from lower to higher NaCl concentration, circular dichroism (CD) is one of the possible methods, although CD has some concern of the negative effect due to the salting-out induced aggregation in the higher salt concentration range, causing the background noise or the decrease of the transmitted light hindered by the aggregation. To acquire the conformational knowledge of the salt effect on FN3 solution from 100 mM to 4.0 M NaCl, CD measurements were carried out. The detail experimental condition was previously described.[36,37]

Figure S13 shows the NaCl concentration dependence of CD spectra of FN3 solution (1.0 mg/mL) at (a) pH 6.0 and (b) 3.0 and (c) the differential spectrum at 100 mM NaCl. As the NaCl concentration increases, the entire spectral intensity decreases, implying that the decrease of the transmitted light intensity due to the salting-out induced by the aggregation or the spectral change caused by the protein conformational change. Figure S13c shows the differential CD spectrum calculated by the subtraction of the spectrum at pH 3.0 from the one at pH 6.0, indicating the conformational difference which is also observed by the Raman differential spectrum (Figure 2).

To clarify the main cause of the salt induced CD spectral change, principal component analysis (PCA) was applied to the NaCl concentration dependent dataset. Figure S14 shows (a, c) the PCA loadings and (b, d) scores at pH 6.0 and 3.0, respectively, showing that only the 1st component is the main one and the others are minor components caused by the spectral noise. The eigenvalue of each dataset also shows that the 1st component is the main factor. Therefore, the salt induced CD spectra decrease without spectral changes, indicating that the salting-out effect can hardly affect the protein secondary structure or can cause only the subtle structural changes, which cannot be observed by the CD

measurement. In this manner, although the good SN ratio of CD measurements cannot be secured due to the salting-out induced aggregation, the conformational knowledge can be partially obtained.

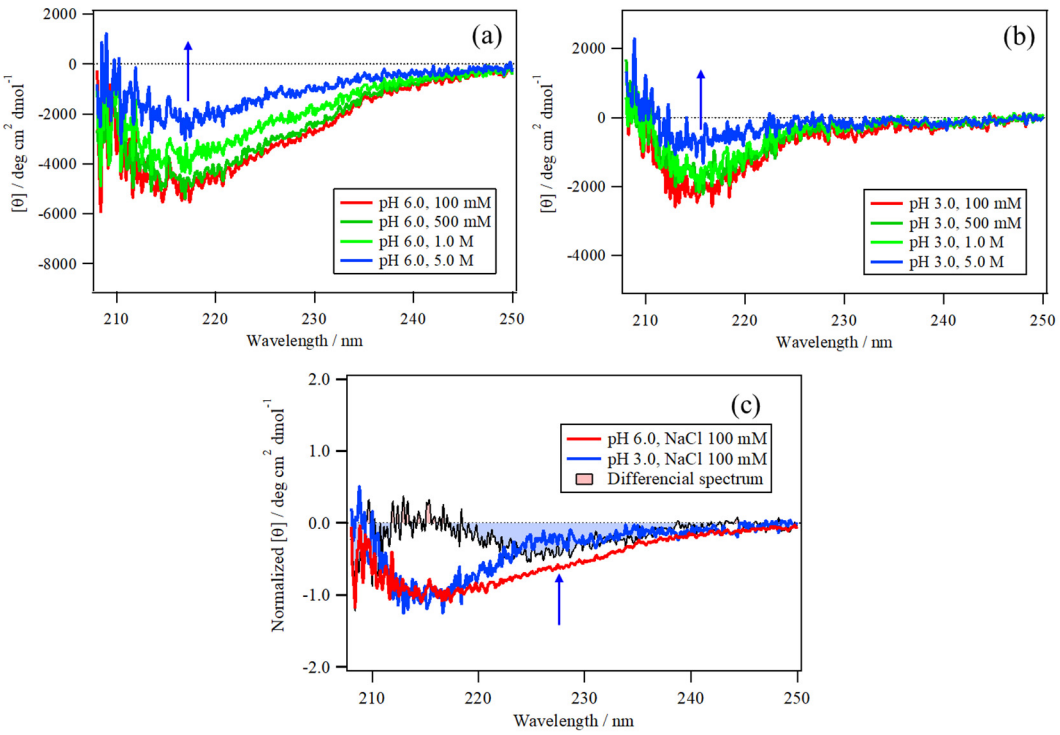

Figure S13. The NaCl concentration dependence of CD spectra of FN3 solution (1.0 mg/mL) at (a) pH 6.0 and (b) 3.0 and (c) the differential spectrum at 100 mM NaCl.

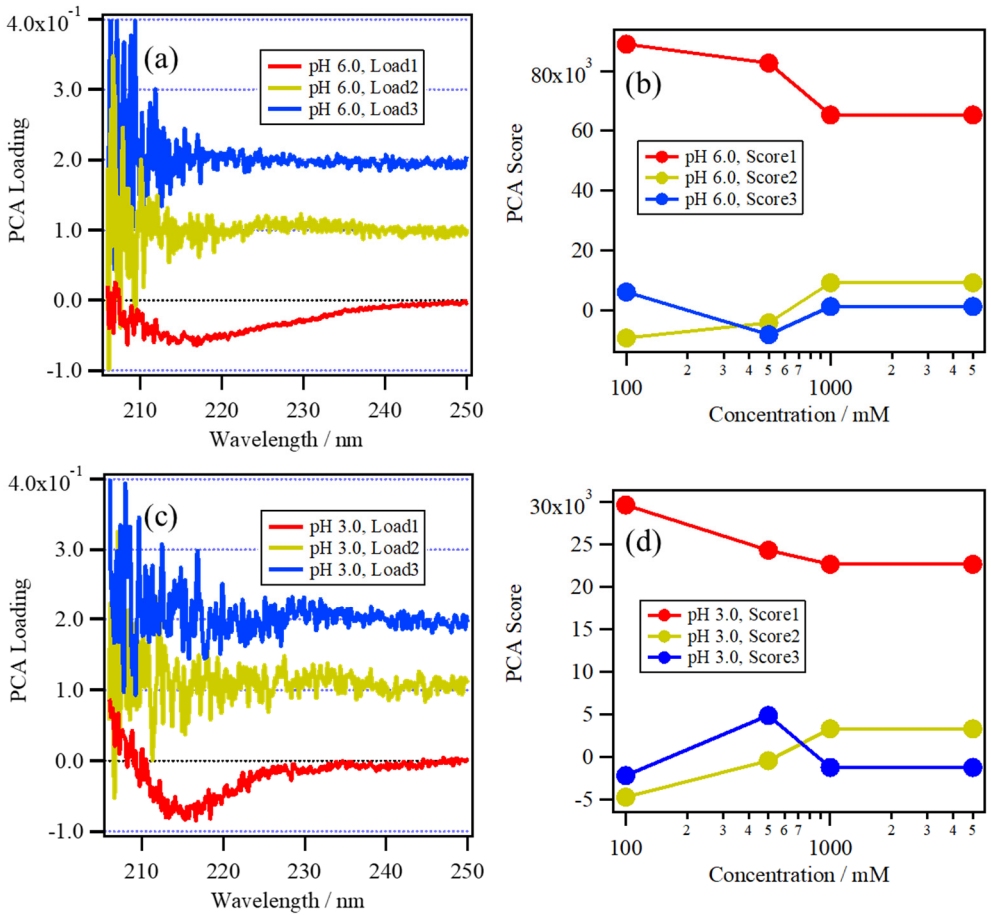

Figure S14. PCA loadings and scores of the NaCl concentration dependent CD spectra of FN3 solution (1.0 mg/mL) at (a, b) pH 6.0 and (c, d) pH 3.0.

REFERENCES

1. Koide, A.; Jordan, M. R.; Horner, S. R.; Batori, V.; Koide, S. Stabilization of a Fibronectin Type III Domain by the Removal of Unfavorable Electrostatic Interactions on the Protein Surface. *Biochemistry* **2001**, *40* (34), 10326–10333.

2. Cota, E.; Steward, A.; Fowler, S. B.; Clarke, J. The Folding Nucleus of a Fibronectin Type III Domain Is Composed of Core Residues of the Immunoglobulin-like Fold. *J. Mol. Biol.* **2001**, *305* (5), 1185–1194.

3. Cota, E.; Hamill, S. J.; Fowler, S. B.; Clarke, J. Two Proteins with the Same Structure Respond Very Differently to Mutation: The Role of Plasticity in Protein Stability. *J. Mol. Biol.* **2000**, *302* (3), 713–725.

4. Takeuchi, H. UV Raman Markers for Structural Analysis of Aromatic Side Chains in Proteins. *Anal. Sci.* **2011**, *27* (11), 1077.

5. Kocherbitov, V.; Latynis, J.; Misiunas, A.; Barauskas, J.; Niaura, G. Hydration of Lysozyme Studied by Raman Spectroscopy. *J. Phys. Chem. B* **2013**, *117* (17), 4981–4992.

6. López-Peña, I.; Leigh, B. S.; Schlamadinger, D. E.; Kim, J. E. Insights into Protein Structure and Dynamics by Ultraviolet and Visible Resonance Raman Spectroscopy. *Biochemistry* **2015**, *54* (31), 4770–4783.

7. Fischer, W. B.; Eysel, H. H. Polarized Raman Spectra and Intensities of Aromatic

Amino Acids Phenylalanine, Tyrosine and Tryptophan. *Spectrochim. Acta Part A Mol. Spectrosc.* **1992**, *48* (5), 725–732.

8. Pflüger, F.; Hernández, B.; Ghomi, M. Vibrational Analysis of Amino Acids and Short Peptides in Hydrated Media. VII. Energy Landscapes, Energetic and Geometrical Features of l-Histidine with Protonated and Neutral Side Chains. *J. Phys. Chem. B* **2010**, *114* (27), 9072–9083.

9. Hernández, B.; Pflüger, F.; Kruglik, S. G.; Ghomi, M. Characteristic Raman Lines of Phenylalanine Analyzed by a Multiconformational Approach. *J. Raman Spectrosc.* **2013**, *44* (6), 827–833.

10. Hernández, B.; Coïc, Y.-M.; Pflüger, F.; Kruglik, S. G.; Ghomi, M. All Characteristic Raman Markers of Tyrosine and Tyrosinate Originate from Phenol Ring Fundamental Vibrations. *J. Raman Spectrosc.* **2016**, *47* (2), 210–220.

11. McHale, J. L. Fermi Resonance of Tyrosine and Related Compounds. Analysis of the Raman Doublet. *J. Raman Spectrosc.* **1982**, *13* (1), 21–24.

12. Pflüger, F.; Hernández, B.; Ghomi, M. Vibrational Analysis of Amino Acids and Short Peptides in Hydrated Media. VII. Energy Landscapes, Energetic and Geometrical Features of l -Histidine with Protonated and Neutral Side Chains. *J. Phys. Chem. B* **2010**, *114* (27), 9072–9083.

13. Hernández, B.; Pflüger, F.; Adenier, A.; Kruglik, S. G.; Ghomi, M. Vibrational Analysis of Amino Acids and Short Peptides in Hydrated Media. VI. Amino Acids with Positively Charged Side Chains: L-Lysine and L-Arginine. *J. Phys. Chem. B* **2010**, *114* (46), 15319–15330.

14. Alex A. Granovsky, Firefly version 8, www http://classic.chem.msu.su/gran/firefly/index.html.

15. Schmidt, M. W.; Baldridge, K. K.; Boatz, J. A.; Elbert, S. T.; Gordon, M. S.; Jensen, J. H.; Koseki, S.; Matsunaga, N.; Nguyen, K. A.; Su, S.; et al. General Atomic and Molecular Electronic Structure System. *J. Comput. Chem.* **1993**, *14* (11), 1347–1363.

16. Siamwiza, M. N.; Lord, R. C.; Chen, M. C.; Takamatsu, T.; Harada, I.; Matsuura, H.; Shimanouchi, T. Interpretation of the Doublet at 850 and 830 cm^{-1} in the Raman Spectra of Tyrosyl Residues in Proteins and Certain Model Compounds. *Biochemistry* **1975**, *14* (22), 4870–4876.

17. Zhang, Y.; Cremer, P. S. The Inverse and Direct Hofmeister Series for Lysozyme. *Proc. Natl. Acad. Sci. U. S. A.* **2009**, *106* (36), 15249–15253.

18. Chen, X.; Yang, T.; Kataoka, S.; Cremer, P. S. Specific Ion Effects on Interfacial Water Structure near Macromolecules. *J. Am. Chem. Soc.* **2007**, *129* (40), 12272–12279.

19. Laage, D.; Elsaesser, T.; Hynes, J. T. Water Dynamics in the Hydration Shells of

Biomolecules. *Chem. Rev.* **2017**, *117* (16), 10694–10725.

20. Ota, C.; Takano, K. Behavior of Bovine Serum Albumin Molecules in Molecular Crowding Environments Investigated by Raman Spectroscopy. *Langmuir* **2016**, *32* (29), 7372–7382.

21. Gasymov, O. K.; Glasgow, B. J. ANS Fluorescence: Potential to Augment the Identification of the External Binding Sites of Proteins. *Biochim. Biophys. Acta - Proteins Proteomics* **2007**, *1774* (3), 403–411.

22. Matulis, D.; Lovrien, R. 1-Anilino-8-Naphthalene Sulfonate Anion-Protein Binding Depends Primarily on Ion Pair Formation. *Biophys. J.* **1998**, *74* (1), 422–429.

23. Ory, J. J.; Banaszak, L. J. Studies of the Ligand Binding Reaction of Adipocyte Lipid Binding Protein Using the Fluorescent Probe 1, 8-Anilinonaphthalene-8-Sulfonate. *Biophys. J.* **1999**, *77* (2), 1107–1116.

24. Lartigue, A.; Gruez, A.; Spinelli, S.; Rivière, S.; Brossut, R.; Tegoni, M.; Cambillau, C. The Crystal Structure of a Cockroach Pheromone-Binding Protein Suggests a New Ligand Binding and Release Mechanism. *J. Biol. Chem.* **2003**, *278* (32), 30213–30218.

25. Lartigue, A.; Gruez, A.; Spinelli, S.; Rivière, S.; Brossut, R.; Tegoni, M.; Cambillau, C. The Crystal Structure of a Cockroach Pheromone-Binding Protein Suggests a New Ligand Binding and Release Mechanism. *J. Biol. Chem.* **2003**, *278* (32), 30213–30218.

26. Grosdidier, A.; Zoete, V.; Michielin, O. SwissDock, a Protein-Small Molecule Docking Web Service Based on EADock DSS. *Nucleic Acids Res.* **2011**, *39* (SUPPL. 2), 270–277.

27. Grosdidier, A.; Zoete, V.; Michielin, O. Fast Docking Using the CHARMM Force Field with EADock DSS. *J. Comput. Chem.* **2011**, *32* (10), 2149–2159.

28. Haberthür, U.; Caflisch, A. FACTS: Fast Analytical Continuum Treatment of Solvation. *J. Comput. Chem.* **2008**, *29* (5), 701–715.

29. Nittinger, E.; Flachsenberg, F.; Bietz, S.; Lange, G.; Klein, R.; Rarey, M. Placement of Water Molecules in Protein Structures: From Large-Scale Evaluations to Single-Case Examples. *J. Chem. Inf. Model.* **2018**, *58* (8), 1625–1637.

30. Mahmoud, A. H.; Masters, M. R.; Yang, Y.; Lill, M. A. Elucidating the Multiple Roles of Hydration for Accurate Protein-Ligand Binding Prediction via Deep Learning. *Commun. Chem.* **2020**, *3* (1), 19.

31. Liu, Y.; Grimm, M.; Dai, W. tao; Hou, M. chun; Xiao, Z. X.; Cao, Y. CB-Dock: A Web Server for Cavity Detection-Guided Protein–Ligand Blind Docking. *Acta Pharmacol. Sin.* **2020**, *41* (1), 138–144.

32. Royer, C. A. Probing Protein Folding and Conformational Transitions with

Fluorescence. *Chem. Rev.* **2006**, *106* (5), 1769–1784.

33. Schmid, F.; Beer, L. Biological Macromolecules : Spectrophotometry Concentrations. *Methods* **2001**, 1–4.

34. Zhdanova, N. G.; Shirshin, E. A.; Maksimov, E. G.; Panchishin, I. M.; Saletsky, A. M.; Fadeev, V. V. Tyrosine Fluorescence Probing of the Surfactant-Induced Conformational Changes of Albumin. *Photochem. Photobiol. Sci.* **2015**, *14* (5), 897–908.

35. Ota, C.; Takano, K. Spectroscopic Analysis of Protein-Crowded Environments Using the Charge-Transfer Fluorescence Probe 8-Anilino-1-Naphthalenesulfonic Acid. *ChemPhysChem* **2019**, *20* (11), 1456–1466.

36. Okada, J.; Koga, Y.; Takano, K.; Kanaya, S. Slow Unfolding Pathway of Hyperthermophilic Tk-RNase H2 Examined by Pulse Proteolysis Using the Stable Protease Tk-Subtilisin. *Biochemistry* **2012**, *51* (45), 9178–9191.

37. Tadokoro, T.; Kazama, H.; Koga, Y.; Takano, K.; Kanaya, S. Investigating the Structural Dependence of Protein Stabilization by Amino Acid Substitution. *Biochemistry* **2013**, *52* (16), 2839–2847.